Electronic Supplementary information

Strain-induced effects in the electronic and spin properties of a monolayer of ferromagnetic $GdAg_2$

Alexander Correa[1,2,3], *Bin Xu*[4,5,6], *Matthieu J. Verstraete* [4,5] , *Lucia Vitali*[1,3,7]

[1] Departamento de física de materiales, Universidad del País Vasco, 20018 San Sebastian (Spain)

[2] Donostia International Physics Center, 20018 San Sebastian (Spain)

3 Centro de Fisica de Materiales (CSIC-UPV/EHU) y Material Physics Center, 20018 San Sebastian (Spain)

[4] CESAM and Département de Physique, Université de Liège, B-4000 Sart Tilman, Belgium

[5] European Theoretical Spectroscopy Facility (http://www.etsf.eu)

[6] Department of Physics and Institute for Nanoscience and Engineering, University of Arkansas, Fayetteville, Arkansas 72701, USA

[7] Ikerbasque Foundation for Science, 48013 Bilbao (Spain)

ESI1. $GdAg_2$ lattice structure

The $GdAg_2$ is a stoichiometric alloy, whose structure closely resembles the previously reported $GdAu_2$ [1]. Following this, a model is sketched in Figure ESI1. The topmost layer is a honeycomb lattice (red line) delimited by silver atoms and centered around one gadolinium atom. The orange rhombus delimits the unit cell of the alloy, whose size is given by the distance between the Gd atoms.

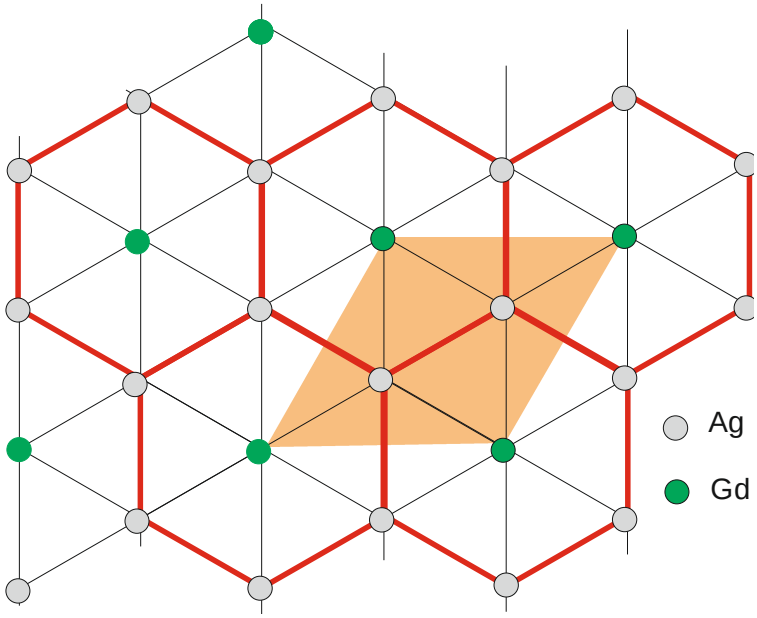

Figure ESI1. Sketch model of the chemical structure of the $GdAg_2$ alloy. Green and gray circles represent the gadolinium (Gd) and the silver (Ag) atoms in the layer. The unit cell of the structure, which contains one Gd atom and two Ag atoms, is drawn in orange.

In order to form this structure gadolinium atoms are evaporated in ultrahigh vacuum on the Ag(111) previously prepared by cycles of Ar+ ion sputtering and subsequent annealing. The Ag(111) surface held at a temperature between 280º and 320ºC to obtain an ordered $GdAg_2$ alloy. At a lower temperature ~240ºC the hexagonal phase predominantly forms. After the preparation the sample was transferred into the STM where the surface was measured at a temperature of 77K, if not otherwise stated.

S2. Modeling details

The electronic structures of $GdAg_2$ alloys are studied by density functional theory (DFT) as implemented in the ABINIT open source package.[2,3] A plane wave basis set (plane wave energy cut off of 20 Hartree) is used with the projector augmented wave (PAW) method[4] to abstract the core states. PAW datasets were generated with the ATOMPAW code[5] (11 valence electrons for Ag, and 18 for Gd). The spin orbit coupling is included in the standard way, perturbatively on the PAW orbitals. The local density approximation (LDA) for the exchange correlation energy was employed. The f-electron states of Gd are extremely localized and strongly correlated: in order to represent them correctly we go beyond (semi)local DFT. Here the LDA+U technique is used,[6] with a Hubbard U parameter of 6.7~eV and J of 0.7~eV, which fixes the Gd f states about 9 eV below the Fermi level. The substrate for the alloy monolayer is modeled as a 7-layer Ag (111) slab with the in-plane lattice constant of the relaxed bulk of Ag (2.83 Å). The alloy layer and two Ag sublayers were relaxed.

The treatment of the incommensurate moiré of the alloy overlayer structure is a crucial point to compare with experiment. The experimental alloy structure has a long-range periodicity, giving rise to a moiré pattern. This structure is simulated in DFT using a commensurate approximant: the $\sqrt{3}\times\sqrt{3}$ supercell cell of the noble metal (111) surface is overlaid with the alloy unit cell. The in-plane lattice constant is fixed to the relaxed bulk DFT value (2.83 Å) for Ag. The strain compared to experiment (imposed by commensurability) is quite large: 8%. The substrate is modeled as a slab of 7 layers of Ag, constructed along the (111) direction. A minimum of 11 Å of vacuum was used to separate the slabs, in order to avoid interference between periodic images. The structures were relaxed for the alloy and the top three layers of substrate atoms, until forces were below 2×10^{-3} Ha/bohr. In several instances, we checked that the differences in the electronic properties (band structure) are negligible compared to structures converged to maximum forces of less than 10^{-5} Ha/bohr.

The incommensurability of the experimental primitive surface unit cells implies that, along the moiré pattern, the alloy is centered at different positions of the $\sqrt{3}\times\sqrt{3}$ substrate. We study the three representative shifts through which the system must pass, where the alloy atoms fall either in the “natural” fcc positions, in the hcp positions with respect to the last two layers of substrate, or on top of surface atoms (top). The three will recur periodically in the moiré pattern. We will see below that fcc and hcp share most properties but that the top position is quite different in bonding and electronic

structure. Because of the lattice mismatch and strain, the electronic bands of the surface alloy and subsurface noble metal layer are shifted in energy. Based on tests with variable lattice parameters, the shifts are not homogeneous for all of the bands linked to a given layer. Further, the charge transfer between the alloy and surface will also depend on the strain, and will give a relative shift of the alloy bands with respect to the bulk noble metal bands. Finally, it is well known that the unoccupied Kohn-Sham energies are not quantitatively accurate predictions of band positions. As a result, the comparison of bands with experimental STS features in the following will be qualitative, and used to explain their nature, relative positions, and dependency on alloy position and magnetization.

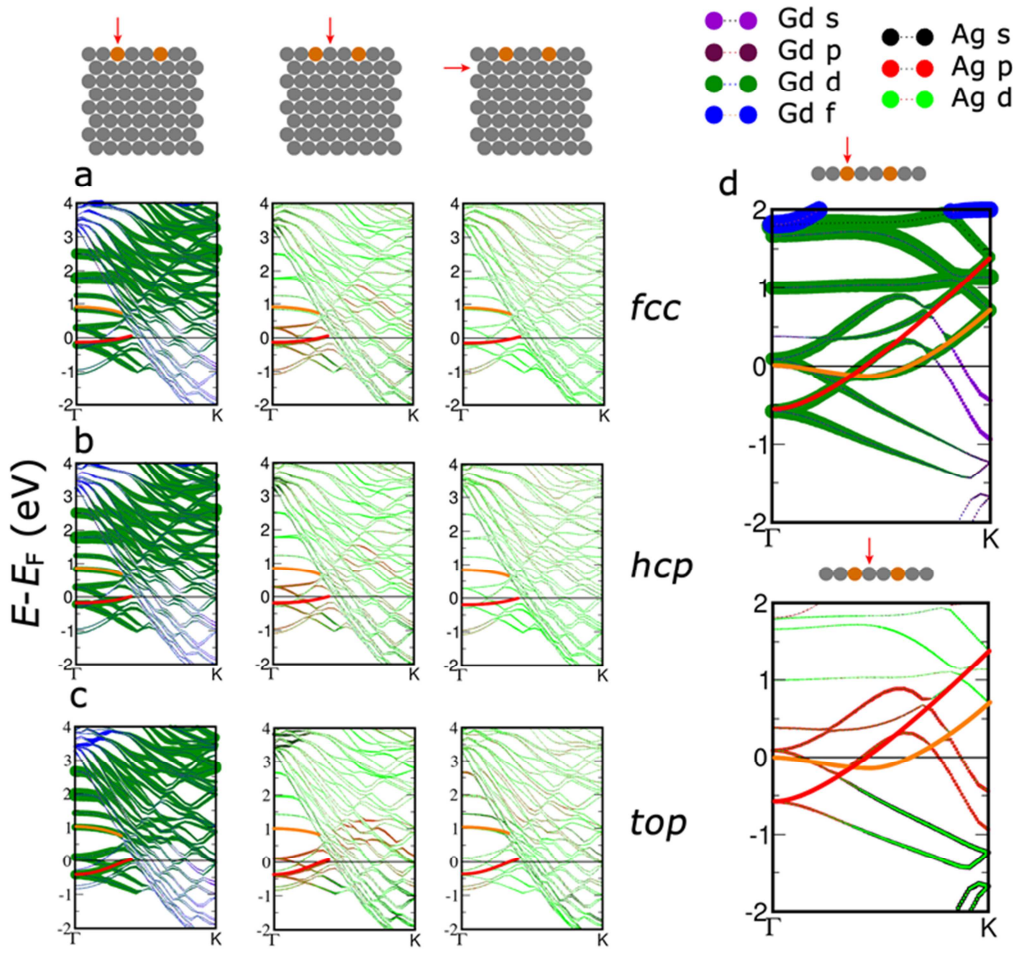

Figure ESI2. Comparison of the electronic band structures between $GdAg_2$ alloy on Ag substrate and free standing $GdAg_2$ monolayer with the theoretically relaxed lattice constant. (a-c). Calculated band structures of alloy with substrate for fcc, hcp, and top configurations. Colors and line width denote the contributions from different orbitals of Gd and Ag atoms (in the alloy layer and the first sublayer). (d) Calculated band structures of the free-standing alloy monolayer. The magnetization is in-plane. The main bands that are observed in STS are highlighted with solid red and orange lines.

Figure ESI2 compares the electronic states for different layer stackings (hcp, fcc, top) with those of the free-standing alloy layer. In each case, the atomic orbital projections on Gd and Ag (as well as the first layer of substrate) are shown, and the two bands visible in STM/STS are highlighted in orange and red.

Figure ESI3 shows the weak effect of magnetic moment orientation on the electron band structure, in the three stackings. All cases are topologically similar, with a shift down in bands near the Fermi level for the top stacking. Some band splittings can be observed in the out-of-plane case, e.g. around 2eV at the Gamma point for top stacking.

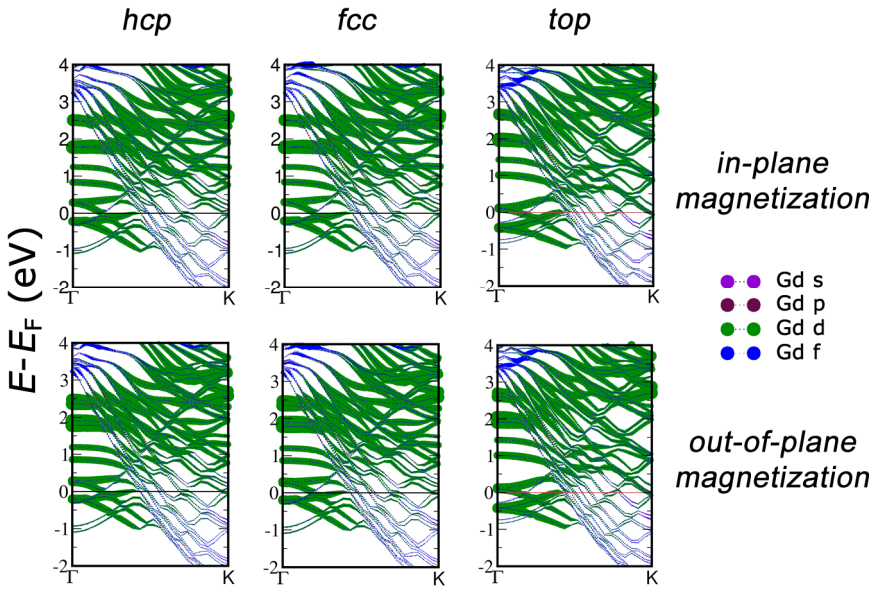

Figure ESI3. Calculated band structures for three relative positions of the $GdAg_2$ alloy with respect to the substrate, including spin-orbit coupling. Three columns from left to right are hcp, fcc, and top configurations. The top row is for in-plane magnetization, and the bottom row is for out-of-plane magnetization.

The Gd-d orbital character of the electronic bands near the Fermi level is shown in Figure ESI4 for the free standing alloy layer. Each pair of spin-orbit split bands has a specific orbital character, with the crucial bands near E_F being in-plane d_{xy} and $d_{x^2-y^2}$, as could be expected from hybridization arguments with the Ag in plane. The differentiation between d_{yz} and d_{xz} orbitals is due to the hexagonal lattice symmetry, which breaks their equivalence.

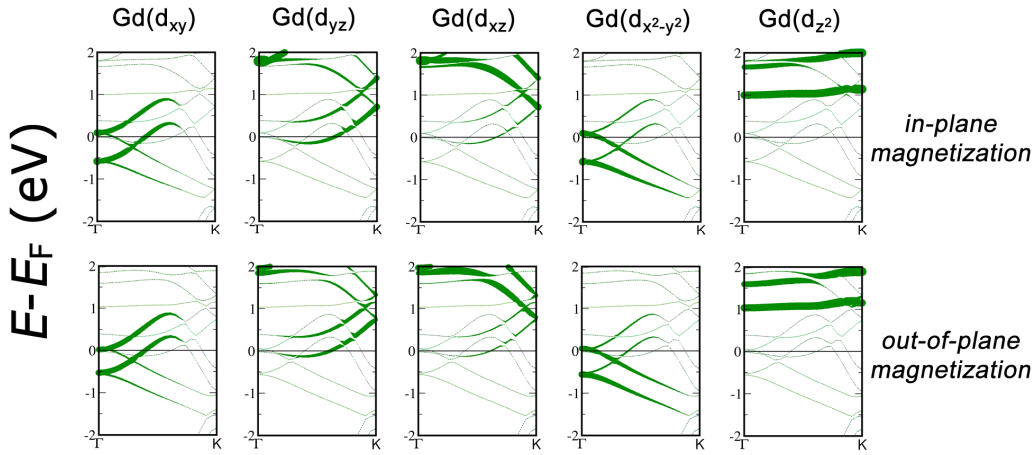

Figure ESI4. Calculated Gd 5*d* orbital contributions in the $GdAg_2$ free standing alloy layer, for in-plane and out-of-plane magnetization.

In Table ESI1 we show the magnetic anisotropy of isolated monolayers with changing strain conditions. The order remains the same as in the supported case, and the anisotropy is almost independent of strain.

Magnetization	$E_{out\text{-}of\text{-}plane} - E_{in\text{-}plane}$			
Lattice constant (Å)	4.91	5.247	5.3	5.5
Anisotropy (meV)	157	175	180	186

Table ESI1. **The calculated out-of-plane magnetic anisotropy ($E_{out\text{-}of\text{-}plane} - E_{in\text{-}plane}$) of the free standing monolayer alloy, with respect to lattice constant.** The energies are in meV per formula unit of alloy, and relative to the lowest energy configuration for each case. Note that much smaller in-plane anisotropy exists as well, and determines the Curie temperature of the system: the out-of-plane anisotropy is a signature of the overall magnetic strength of the FM state. As with the supported case in Table 2 of the main text, the easy axis is in-plane.

ESI3. Density of states on GdAg2 superstructure

The density of states that characterizes the apparent hills and valleys of the $GdAg_2$ moiré superstructure is shown in figure ESI5a as red and green line, respectively. The localization of the spectroscopic features is evident by comparing topographic image and energy maps measured at the energy of the peaks observed in the dI/dV spectra.

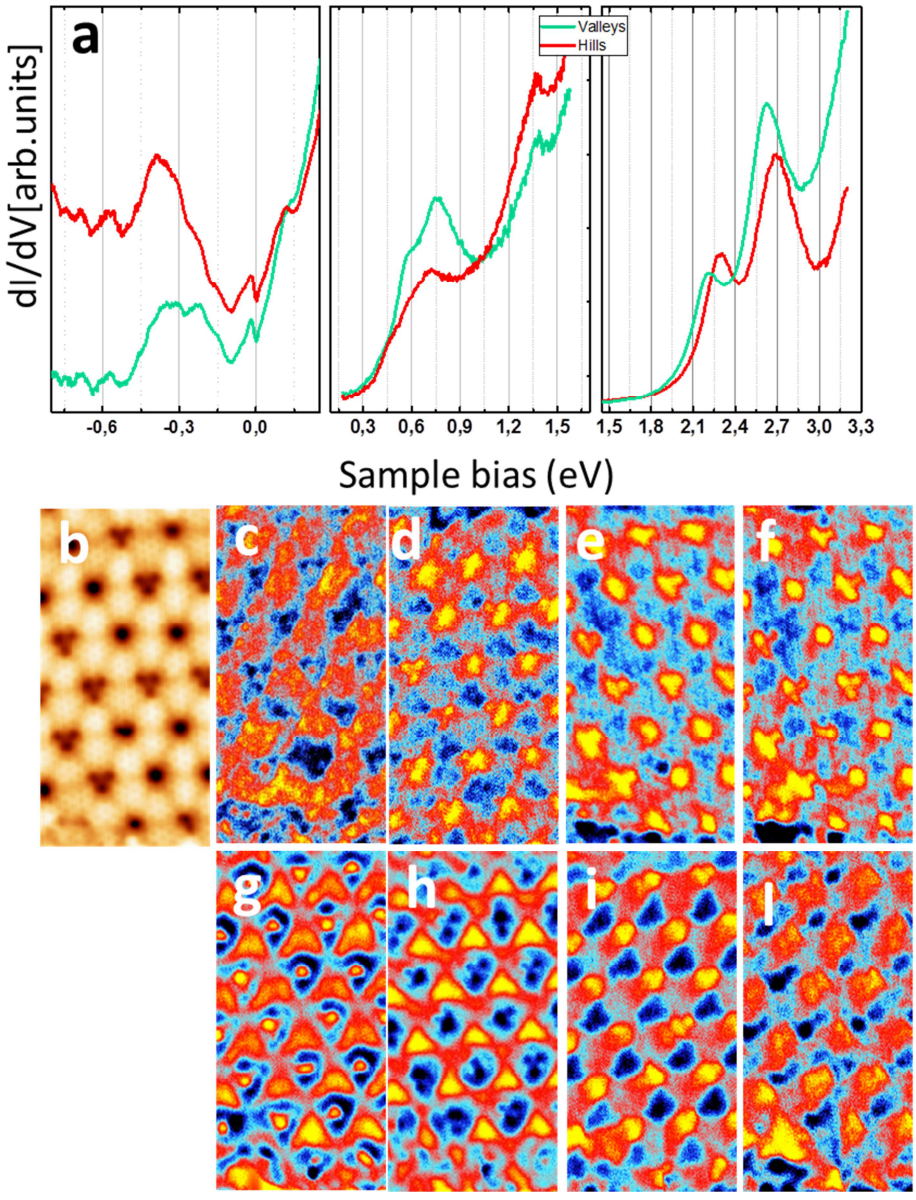

Figure ESI5. Topographic image and the density of states measured on different position of the GdAg2 moiré superstructure at the temperature of 1K (a) dI/dV spectra on hills and valley position of the moiré superstructure (b) measured at (c). -300meV, (d) -200meV; (e) 600meV, (f) 790meV, (g) 2.2eV; (h) 2.3eV; (i) 2.6eV; (l) 2.7eV.

ESI4. Density of states on the "hills" position of the moiré patterns

A comparison of the density of states measured on the two moiré patterns shown in Figure 1 of the main text (hills positions), is reported in Figure ESI6. The spectra are shown in separate panels for a better visualization. Spectroscopic differences between two moiré patterns are found in the whole range of density of states. These characterize each of the two moiré pattern as evinced by the energy maps achieved on the topographic image (panels b-h)

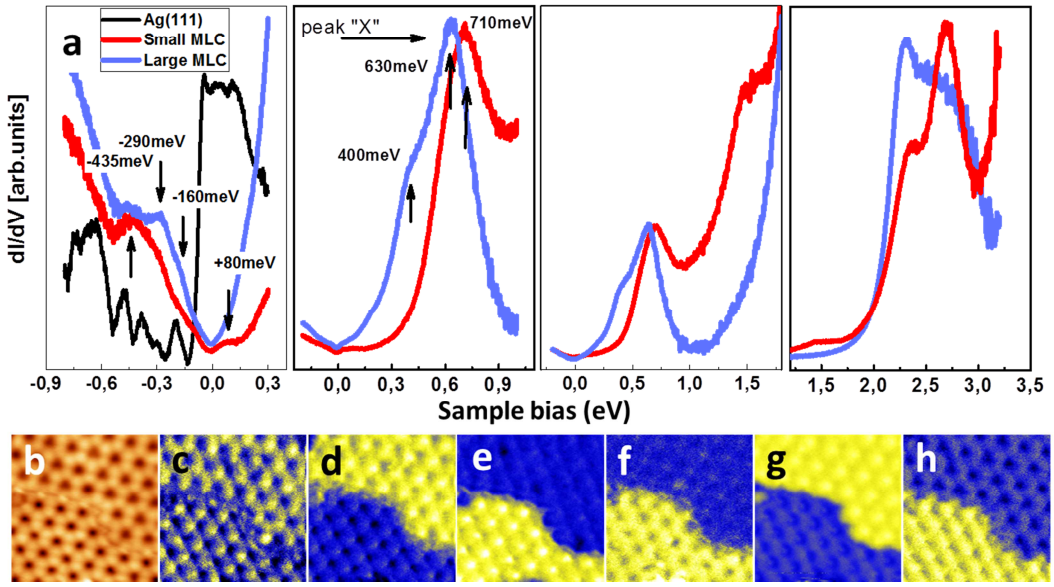

Figure ESI6. The LDOS and conductance maps measured on the "hill" position of two differing moiré super-structures of $GdAg_2$. (a) dI/dV spectra. (b) Topographic image. (c-h) Conductance maps at the energy corresponding to the features in the density of states (c). -280meV, (d). 380meV, (e). 700meV; (f). 1.4eV; (g). 2.2 eV; (h). 2.7eV.

ESI5. Density of states on the “dark” position of the moiré patterns

The local densities of states measured on the “valley” positions of the two moiré patters are reported in Figure ESI6.

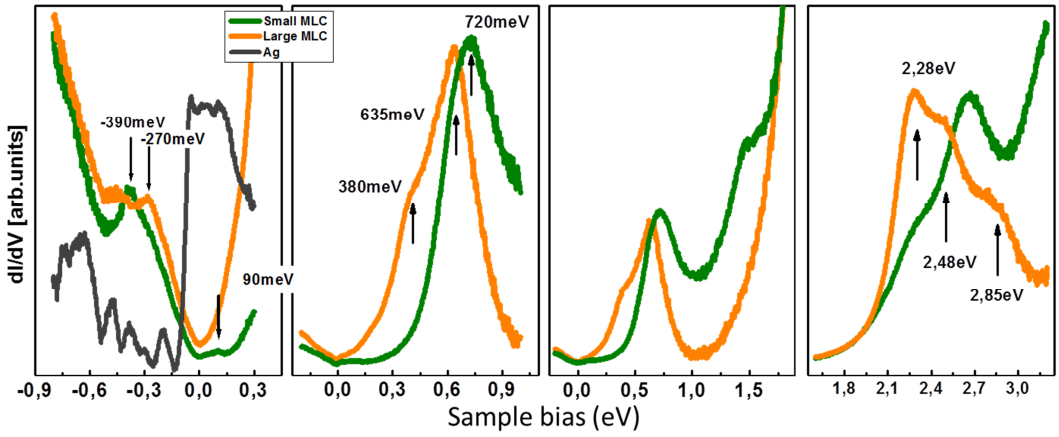

Figure ESI7. LDOS measured on the valley positions of the moiré superstructures of $GdAg_2$. dI/dV spectra have been achieved on the small and large moiré super-lattice constants (SMLC, LMLC)

ESI6. Moiré superstructures of $GdAg_2$ on Ag(111)

High resolution image of two moiré superstructures of the $GdAg_2$ monolayer alloy grown on Ag(111) are shown in Figure ESI8. The white lines highlight that these differ in periodicity and relative orientation. Atomically resolved images of the two superstructures (panel b and c) show that the alloy unit cell (small black rhombus) is also rotated of an angle γ with respect to the unit cell of the superstructures (white rhombus). The lattice constant of the $GdAg_2$ unit cell, 5.15±0.05Å and 5.25±0.05Å, and the angle of rotation γ characterize these structures.

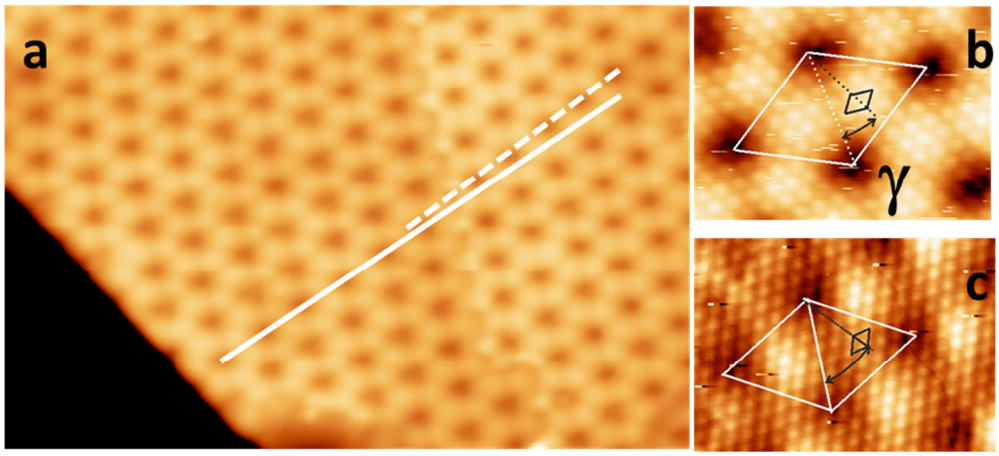

Figure ESI8. $GdAg_2$ moiré structures on Ag(111). (a) Topographic image of one monolayer of $GdAg_2$ alloy on Ag(111) showing two moiré structures (230x150Å). The white lines underline the relative rotation of the two moiré patterns. (b and c) Atomic resolution of the two moiré patterns achieved on the left and on the right superstructure of panel a, respectively. The white and black rhombi show that $GdAg_2$ lattice has a different orientation on the two moiré patterns.

ESI7 Lattice constant estimation

Moiré superstructures are envisioned as the superposition of two incommensurate layers, as for example, an overlayer and a supporting substrate, and/or by their relative rotations. Each combination of different lattice constants and angle of rotation leads to a moiré superstructure with different characteristics as periodicity and angle of rotation. The lattice constant, the relative orientation of the overlayer, in the present case of $GdAg_2$ alloy, can be calculated using the coincidence model described by Hermann[7] with the parameters of the substrates Ag(111) and/ or of the moiré superstructures.

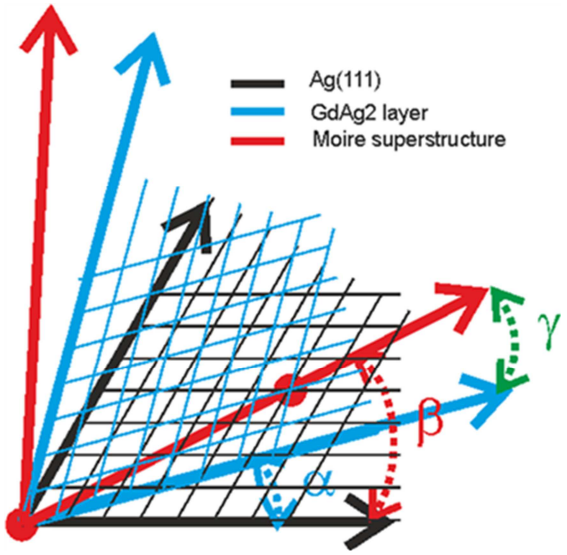

Figure ESI9 Scheme of the coincidence lattice model. The alloy lattice (blue) is superimposed on the substrate (black) and generates a coincidence networks (red) that forms the moiré pattern.

The lattice of $GdAg_2$ (blue) and Ag(111) (black) differs in unit cell size and form a relative angle of rotation α. The coincidence network is formed by the atoms of the alloy layer superposing on atoms of the Ag(111) substrate. This defines the orientation and lattice constant of the moiré superstructure which is characterized by an angle β with respect to the substrate and an angle γ with respect to the alloy layer. The experimentally observed angle γ is shown in Figure ESI8.

According to this model, the periodicity of the superstructure follows the following relation:

1.

$$M = \frac{a}{\sqrt{\left(1 + \left(\frac{a}{b}\right) * \left(\frac{a}{b}\right) - 2\left(\frac{a}{b}\right)\cos(\alpha)\right)}}$$

where *a* and *b* are respectively the lattice constants of Ag(111) and the first nearest neighbor distance in the alloy layer. The angle α defines the relative orientation between the alloy layer and Ag(111). The angle β between the moiré superstructure and the supporting substrate can be calculated as follows:

2. $\beta = \arccos\left(\frac{\cos(\alpha)-\left(\frac{a}{b}\right)}{\sqrt{1+\left(\frac{a}{b}\right)*\left(\frac{a}{b}\right)-2\left(\frac{a}{b}\right)\cos(\alpha)}}\right)$

The angle γ is the angle between the moiré superstructure and the alloy layer and can be related to α and β by the simple equation:

3. $\gamma=\beta-\alpha$

Using this model, fixing only the substrate lattice constant to 2.9Å, we have calculated the possible combinations of first atom nearest neighbor distance *b* in the alloy and relative rotation angle α with respect to Ag(111) which lead to the periodicities of moiré superstructures experimentally observed. Among the possible parameters calculated for this system we report in Table 1 the ones that reproduce the experimentally observed superstructure.

	Experimentally observed		Values expected[1]	
moiré periodicity *M*	32Å	34Å	32.12±0.1Å	34.2±0.1Å
Rotation angle γ	28±1º	20±1º	28.7±0.1º	20.9±0.1º
Atomic distance between Gd atoms	5.23±0.2Å	5.13±0.2Å	5.247±0.001Å	5.156±0.001Å
First nearest neighbor's distance			3.033Å	2.981Å
Rotation angle β			3.1±0.2 º	13.7±0.2º
Rotation angle α			34.6º	34.65º

Table ESI2. Comparison between the experimentally observed values of the moiré super-structures and those calculated using the Hermann model.

References

(1) L.Fernandez, M. Blanco-Rey, M. Ilyn, L. Vitali, A. Magaña, A. Correa, P. Ohresser, E. Ortega, A. Ayuela, F. Schiller,; Nano Letters **2014**, 14, 2977

(2) X. Gonze.; *Zeitschrift für Krist.* 2005, 220, 558

(3) X. Gonze , B. Amadon, P.-M. Anglade, J.-M. Beuken, F. Bottin, P. Boulanger, F. Bruneval, D. Caliste, R. Caracas, M. Côté,T. Deutsch,L. Genovese,Ph. Ghosez, M. Giantomassi, S. Goedecker, D.R. Hamann, P. Hermet, F. Jollet, G. Jomard, S. Leroux, M. Mancini, S. Mazevet, M.J.T. Oliveira, G. Onida, Y. Pouillon, T. Rangel, G.-M. Rignanese, D. Sangalli, R. Shaltaf, M. Torrent, M.J. Verstraete, G. Zerah, J.W. Zwanziger**;** *Comput. Phys. Commun.* 2009, **180,** 2582

(4) P.E. Blöchl, *Phys. Rev. B* **50,** 17953–17979 (1994).

(5) N. A. W. Holzwarth, A.R. Tackett, G.E. Matthews, *Comput. Phys. Commun.* **135,** 329–347 (2001).

(6) V.I. Anisimov, F. Aryasetiawan, A.I. Liechtenstein, *J. Phys. Condens. Matter* **9,** 767–808 (1997).

(7) K. Hermann; *J. Phys*. **2012**, 24, 314210